

See discussions, stats, and author profiles for this publication at: <https://www.researchgate.net/publication/311582448>

Texture Features for Classification of Vascular Ultrasound

Conference Paper · December 2016

CITATIONS

0

READS

326

4 authors, including:



Jordan Smith

Memorial University of Newfoundland

6 PUBLICATIONS 7 CITATIONS

SEE PROFILE



Andrew Smith

Memorial University of Newfoundland

31 PUBLICATIONS 292 CITATIONS

SEE PROFILE

Some of the authors of this publication are also working on these related projects:



Object tracking [View project](#)



Prediction of Congestive Heart Failure Hospitalization [View project](#)

Texture Features for Classification of Vascular Ultrasound

Jordan P. Smith¹, Mohamed S. Shehata¹, Peter F. McGuire², Andrew J Smith³

Abstract—Information regarding a patient’s health status can be extracted from ultrasound imagery of the arterial and venous vasculature. This paper investigates the use of Haralick features and edge features to distinguish euvoolemia from hypovolemia. Transverse ultrasound videos of the internal jugular vein were collected from a set of healthy subjects using a simulation to generate different volume states. Features were extracted from each frame and assessed using common feature selection methods. These features provided a reasonable classification accuracy of 88.6% and worked best when considering texture on a small scale.

Index Terms—internal jugular vein, volume status, classification, ultrasound, Haralick features

I. INTRODUCTION

Ultrasound is becoming an increasingly affordable and compact imaging modality capable of providing rapid and repeatable diagnostics immediately at the patients bedside [10]. With increased use, more data may become available for the development of diagnostic support systems which automatically process images in the attempt to provide additional information to the operator. As a preliminary step, this paper focuses on the use of textural information contained within ultrasound imagery in the prediction of volume status.

Intravascular volume status is an estimate of the volume of fluid within a subject’s circulatory system. Hypovolemia (deficit) or hypervolemia (excess) results in increased morbidity, mortality and hospital length of stay [20] whereas euvoolemia (normal) represents an idealized goal. Changes in central venous pressure (CVP) and circulating blood volume are known to correlate with changes in blood vessels such as the internal jugular vein (IJV)[1], [15]. These vessels change in size, shape and acutance as they become distended or collapse depending on volume status of the patient. In cross section, as in a transverse ultrasound of the neck, the IJV will appear as a contiguous hypoechoic (dark) region surrounded by more hyperechoic (bright) material containing a variety of different textures as shown in figure 1. The appearance of tissues around the vessel, the vessel walls, the lumen and ultrasound artifact change with volume status. For example, as the target vessel collapses, the interior boundary of the vessel becomes indistinct and may be easily lost. However, the vessel walls are still present in the region of interest and the combination of anechoic vessel lumen, wall and surrounding tissue may present a distinct feature when segmentation is difficult.



Figure 1. Transverse ultrasound of the neck depicting the internal jugular vein (marked) beside the internal carotid artery and surrounding soft tissues.

II. DATASET

A simulation was used in this study to mimic changes in a subject’s circulating blood volume. Subject’s position were varied from recumbent to sitting upright using a standard hospital stretcher with the supine position reflecting hypervolemia or euvoolemia and sitting reflecting relative hypovolemia [12], [14]. Ultrasound video clips were recorded in the transverse plane using a linear array transducer (6-15 MHz) and the Sonosite M-Turbo Ultrasound (Sonosite, Bothell, USA). Illustration of the simulation is shown in figure 2.

Two ultrasound videos were recorded for each of 29 healthy subjects to account for some of the diverse inter-subject anatomical and blood volume variability. Also 3 additional subjects were scanned repeatedly over 10 sessions in order to capture intra-subject variability of the circulating blood volume. It is anticipated that error resulting from slight differences in transducer location and applied pressure would be present however efforts to consistently image the same anatomical location on the neck and minimize transducer pressure were taken. Research protocol was reviewed and approved by the Health Research Ethics Authority.

After collection, the region of interest (ROI) was defined for the first frame of each video by an expert segmentation of the IJV. The remaining frames were segmented by an active contours algorithm initialized between frames with optical flow in a method similar to Qian [17] and the results were reviewed by an expert for correctness. Feature selection

¹Computer Engineering Department, Memorial University, St.John’s, Canada {jp.smith, mshehata}@mun.ca

²C-CORE, St.John’s, Canada

³Discipline of Family Medicine, Memorial University, St.John’s, Canada

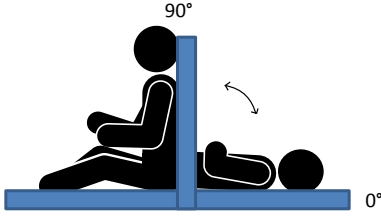


Figure 2. Angles of inclination simulating changes in volume status.

and classification was completed using each frame as an individual sample as vessel motion creates significant change in appearance even within a single video. The training set for feature selection consists of all the frames of both videos for the first 29 subjects for a total of 26100 samples. The training set used the remaining 3 subjects recorded over 10 days for 27000 samples. Figure shows the arrangement of the testing and training data.

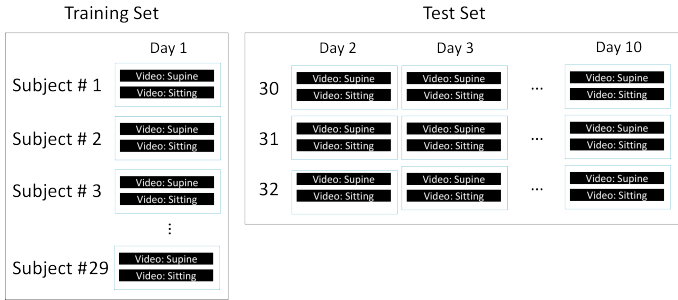


Figure 3. Description of testing and training data.

III. TEXTURE FEATURES

A. Grey Level Co-occurrence Matrices

Grey Level Co-occurrence Matrices (GLCM) have been used for texture identification in many ultrasound applications [22], [23], [25], [11]. Originally devised by Haralick et. al. GLCM displays the spatial relationship between pixels of a given value using a two-dimensional histogram. The nature of the spatial relationship is defined by pixel distance and angle. The angles used for texture description were 0, 45, 90 and 135 degrees. Given the size of speckle noise in the dataset pixel distances which were considered in texture analysis are 1, 2, 3, 5 and 10px.

The GLCM matrix can be computed for any given region and summarized with a single number in a variety of ways[6]. Referring to the formulations used by Scikit-image [21], [13] these are:

$$contrast = \sum_{i,j=0}^{levels-1} P_{i,j}(i-j)^2 \quad (1)$$

$$dissimilarity = \sum_{i,j=0}^{levels-1} P_{i,j}|i-j| \quad (2)$$

$$homogeneity = \sum_{i,j=0}^{levels-1} \frac{P_{i,j}}{1+(i-j)^2} \quad (3)$$

$$angular\ second\ moment\ (ASM) = \sum_{i,j=0}^{levels-1} P_{i,j}^2 \quad (4)$$

$$energy = \sqrt{angular\ second\ moment} \quad (5)$$

$$correlation, C = \sum_{i,j=0}^{levels-1} P_{i,j} \left[\frac{(i-\mu_i)(j-\mu_j)}{\sqrt{(\sigma_i^2)(\sigma_j^2)}} \right] \quad (6)$$

where $P_{i,j}$ is the value of the GLCM matrix at index (i, j) and $levels$ refers to the range of the intensity histogram.

Additional measures include[7]:

$$entropy = \sum_{i,j=0}^{N-1} -P_{ij} \ln(P_{ij}) \quad (7)$$

$$mean, \mu = \sum_{i,j=0}^{N-1} iP_{ij} \quad (8)$$

$$variance, \sigma^2 = \sum_{i,j=0}^{N-1} P_{ij}(i-\mu)^2 \quad (9)$$

$$shade = sign(A) |A|^{1/3} \quad (10)$$

$$where\ A = \sum_{i,j=0}^{N-1} \frac{(i+j-2\mu)^3 P_{ij}}{\sigma^3 (\sqrt{2(1+C)})^3} \quad (11)$$

$$prominence = sign(B) |B|^{1/4} \quad (12)$$

$$where\ B = \sum_{i,j=0}^{N-1} \frac{(i+j-2\mu)^4 P_{ij}}{4\sigma^4 (1+C)^2} \quad (13)$$

Given the variety of options, the number of features under consideration is the product of 6 summary techniques, 5 distances and 4 angles for a total of 120 features per frame.

B. Edge texture descriptors

Ultrasound image quality is tissue, location and depth dependant. When ultrasound is used to image tissue at great depth, sound waves are absorbed and get weaker than at the surface. The resulting loss of energy produces a less defined image unless a lower frequency or higher energy transducer is used. A similar effect on image quality is seen when an abundance of sound absorbing tissue (such as fat) occludes or surrounds a target. As the target vessels change in size and location their edges may change in a measurable way. Three measures of contour acutance (the sharpness across the boundary) can be produced using the image gradient, the image entropy and mean intensity along the boundary [19]. To compute the local entropy, mean and gradient, a small 5 pixel structuring element was applied at all points along the contour and a sum produced from the results.

IV. ANALYSIS

A. Region of Interest

A key consideration in analyzing texture is the size and resolution of the region which is being considered. Three different regions of interest were used in this analysis:

- A naive approach would be to assess the entire active region of the 640x480px ultrasound frame. This active region of 485x375px is considered as a baseline.
- Given that the vessel was identified with an outline in first frame of each video, this region of interest averaging approximately 120x80px may be more appropriate.
- In addition, the actual edge of the vessel can be found using an active contour initialized with the expert outline for the first frame and reinitialized in subsequent frames with the previous frame's contour. This edge is used to compute the 3 edge texture descriptors.

The first analysis included 120 GLCM features computed over the entire 485x375px active region of the frame. The second analysis included 120 GLCM features computed over only the region of interest given by the bounding box of the active contour. The final analysis was identical to the second, but also included 3 edge features along the segmented contour.

B. Feature selection

Filter methods of feature selection pre-screen data and select features before they are passed to a classifier. They are usually based on the statistical properties of the data and work by either ranking features, or suggesting an optimal subset. If a variety of selection methods are used to produce an optimal subset, features which are repeatedly selected are likely to be good features. The resulting selections from several algorithms are shown in Table II. The algorithms used were Correlation-based Feature Selection (CFS)[5], Conditional Infomax Feature Extraction (CIFE)[9], Conditional Mutual Information Maximization (CMIM) [4], Fast Correlation-Based Filter (FCBF) [24], Interaction Capping (ICAP)[8], Mutual Information Feature Selection (MIFS) [2], and Max-Relevance Min-Redundancy (MRMR) [16].

Embedded methods are those which include feature selection as part of training their models. Models built using decision trees include a form of feature selection during training by choosing features which best divide the input data into groups based on variance [3] or entropy reduction [18]. These features and thresholds form the decision nodes of the tree. 'Classification And Regression Trees' can be used to find an optimal number of features as eventually additional branches are found to add no additional information. These features are given weights approaching zero. Features selected with this technique are plotted by their Gini impurities in figure 4.

C. Classifier performance

The embedded feature selection previously described trains a model during the process. The utility of the selected features given in figure 4 is reflected in the accuracy of a classifier which uses them. Table III shows the results of testing the CART classifier on 3 unseen datasets.

Table I
SUBSET SELECTION USING DATASET 1: FEATURES EXTRACTED FROM ENTIRE ACTIVE REGION OF THE ULTRASOUND.

| | CFS | CIFE | CMIM | FCBF | ICAP | MIFS | MRMR |
|-------------------------------|-----|------|------|------|------|------|------|
| ASM, 0degrees, 1px | * | * | * | * | * | * | * |
| energy, 135degrees, 5px | | * | * | | * | | |
| energy, 135degrees, 2px | | | * | | * | | |
| contrast, 135degrees, 1px | | | * | | * | | |
| contrast, 90degrees, 10px | | | * | | * | | |
| dissimilarity, 0degrees, 1px | | * | | | | | * |
| correlation, 0degrees, 2px | | | * | | * | | |
| correlation, 0degrees, 3px | | | * | | * | | |
| ASM, 90degrees, 5px | * | | | | | * | |
| correlation, 135degrees, 10px | | | * | | * | | |
| ASM, 135degrees, 3px | | | * | | * | | |
| correlation, 0degrees, 10px | | | * | | * | | |
| ASM, 0degrees, 10px | * | | | | | | |
| ASM, 90degrees, 3px | * | | | | | | |
| ASM, 45degrees, 1px | * | | | | | | |
| ASM, 45degrees, 5px | * | | | | | | |
| ASM, 45degrees, 2px | * | | | | | | |
| ASM, 135degrees, 2px | * | | | | | | |
| ASM, 135degrees, 1px | * | | | | | | |

Table II
SUBSET SELECTION USING DATASET 3: FEATURES EXTRACTED FROM ROI + EDGE FEATURES.

| | CFS | CIFE | CMIM | FCBF | ICAP | MIFS | MRMR |
|-----------------------------------|-----|------|------|------|------|------|------|
| homogeneity, 90 degrees, 3 px | | * | * | | * | * | * |
| dissimilarity, 135 degrees, 5 px | * | | * | | * | | |
| ASM, 45 degrees, 10 px | | * | * | | * | | |
| homogeneity, 135 degrees, 3 px | | | * | | * | | |
| homogeneity, 135 degrees, 2 px | | | * | | * | | |
| dissimilarity, 0 degrees, 1 px | | | * | | * | | |
| edge intensity | | * | | | | | * |
| ASM, 0 degrees, 2 px | | | * | | * | | |
| ASM, 45 degrees, 5 px | | | * | | * | | |
| dissimilarity, 45 degrees, 3 px | | | * | | * | | |
| dissimilarity, 135 degrees, 10 px | | | * | | * | | |
| correlation, 90 degrees, 10 px | * | | | * | | | |
| edge entropy | | | | | | * | |
| correlation, 45 degrees, 10 px | * | | | | | | |
| correlation, 135 degrees, 10 px | * | | | | | | |
| dissimilarity, 90 degrees, 2 px | * | | | | | | |
| dissimilarity, 90 degrees, 5 px | * | | | | | | |

Table III
CART CLASSIFICATION ACCURACIES USING EACH DATASET

| | 1) Entire frame GLCM | 2) ROI GLCM | 3) ROI + edge |
|-------------------|----------------------|--------------------------|--------------------------|
| test set 1 | 68.67% | test set 1 64.5% | test set 1 88.6% |
| test set 2 | 51.86% | test set 2 61.78% | test set 2 80.10% |
| test set 3 | 61.92% | test set 3 73.35% | test set 3 81.79% |

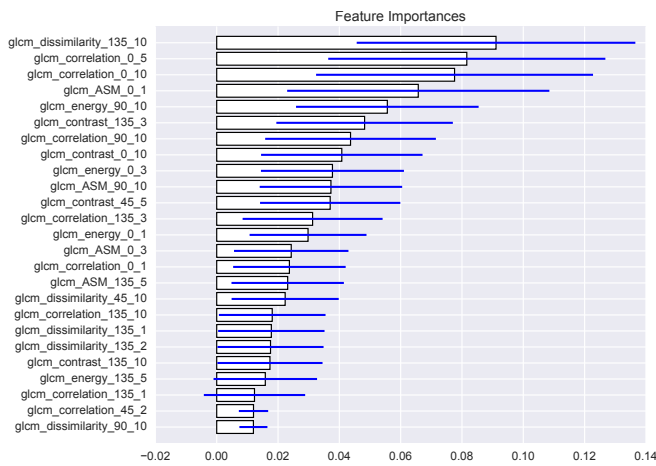


Figure 4. Gini impurities from a CART model trained on the entire frame (dataset 1)

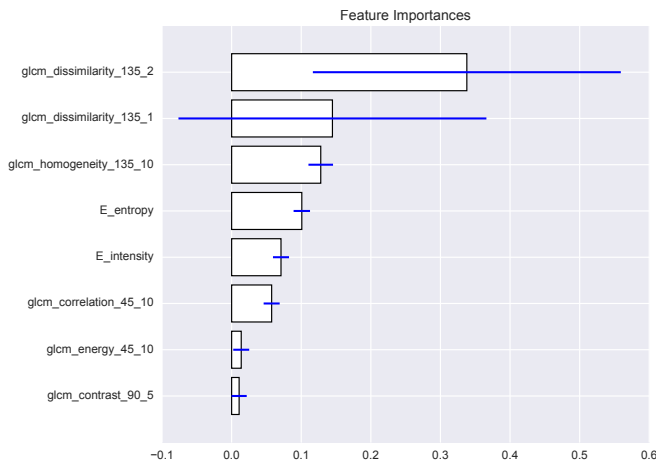


Figure 5. Gini impurities from a CART model trained on only the region of interest around the vessel (dataset 3).

V. DISCUSSION

There is a notable difference in texture between samples of each class even without pre-processing the frame. As focus shifted to the ROI around the vessel, this distinction increased. By processing texture along the edge itself accuracy of a simple decision tree classifier increased by 20% to 28% beyond the baseline.

It is difficult to conclude that any particular distance, angle, or summary formula could be selected over another as the observed gini impurities are quite low in the CART model and there is disagreement between feature selection methods. However it appears smaller distances and the angles ± 45 are preferable.

Mutual information based methods such as CMIM and ICAP roughly agree with each other, but disagree with the merit scores produced by correlation based method CFS. This may mean that classification tasks will prefer different features than regression tasks and that few texture features will be appropriate for both goals.

VI. CONCLUSIONS

A preliminary analysis of GLCM texture features in vascular ultrasound was conducted. Texture features may be a reasonable approach to the classification of vessel state using ultrasound. Classification of subject status may be possible without human pre-processing. A small subset of available texture features were considered and other techniques such as local binary pattern analysis, gabor filter banks or advances in deep learning may produce a much richer feature set allowing high classification rates though the analysis of texture.

REFERENCES

- [1] Christophe Barbier, Yann Loubières, Christophe Schmit, Jan Hayon, Jean-Louis Ricôme, François Jardin, and Antoine Vieillard-Baron. Respiratory changes in inferior vena cava diameter are helpful in predicting fluid responsiveness in ventilated septic patients. *Intensive care medicine*, 30(9):1740–1746, 2004.
- [2] Roberto Battiti. Using mutual information for selecting features in supervised neural net learning. *IEEE Transactions on neural networks*, 5(4):537–550, 1994.
- [3] Hugh A Chipman, Edward I George, and Robert E McCulloch. Bayesian cart model search. *Journal of the American Statistical Association*, 93(443):935–948, 1998.
- [4] François Fleuret. Fast binary feature selection with conditional mutual information. *Journal of Machine Learning Research*, 5(Nov):1531–1555, 2004.
- [5] Mark A Hall. *Correlation-based feature selection for machine learning*. PhD thesis, The University of Waikato, 1999.
- [6] Robert M Haralick, Karthikeyan Shanmugam, et al. Textural features for image classification. *IEEE Transactions on systems, man, and cybernetics*, (6):610–621, 1973.
- [7] Dong-Chien He, Li Wang, and Jean Guibert. Texture discrimination based on an optimal utilization of texture features. *Pattern Recognition*, 21(2):141–146, 1988.
- [8] Aleks Jakulin. *Machine learning based on attribute interactions*. PhD thesis, Univerza v Ljubljani, 2005.
- [9] Dahua Lin and Xiaoou Tang. Conditional infomax learning: an integrated framework for feature extraction and fusion. In *European Conference on Computer Vision*, pages 68–82. Springer, 2006.
- [10] James Milne, Paul Atkinson, Justin Bowra, Osama Loubani, Bob Jarman, and Andrew Smith. My patient is short of breath: is the problem in the lung tissue? *Ultrasound*, 21(2):82–87, 2013.
- [11] Delia Mitrea, Mihai Socaciu, Radu Badea, and Adela Golea. Texture based characterization and automatic diagnosis of the abdominal tumors from ultrasound images using third order glcm features. In *Image and Signal Processing (CISP), 2011 4th International Congress on*, volume 3, pages 1558–1562. IEEE, 2011.
- [12] Akira Morimoto, Izumi Takase, Yukio Shimizu, and Katsuji Nishi. Assessment of cervical venous blood flow and the craniocervical venous valve using ultrasound sonography. *Legal Medicine*, 11(1):10–17, jan 2009.
- [13] Juan Nunez-Iglesias. Scikit-image dev docs: Feature module, 2016.
- [14] Mikhailova Om, Dundukov Nn, Perlei Ve, and Lebedev Na. Effect of various types of sports on the anatomy of the common carotid artery and the internal jugular vein. *Arkhiv anatomii, gistologii i embriologii*, 95(10):47–50, oct 1988.
- [15] Pierpaolo Pellicori, Anna Kallvikbacka-Bennett, Riet Dierckx, Jufen Zhang, Paola Putzu, Joe Cuthbert, Vennela Boyalla, Ahmed Shoaib, Andrew L Clark, and John GF Cleland. Prognostic significance of ultrasound-assessed jugular vein distensibility in heart failure. *Heart*, 101(14):1149–1158, 2015.
- [16] Hanchuan Peng, Fuhui Long, and Chris Ding. Feature selection based on mutual information criteria of max-dependency, max-relevance, and min-redundancy. *IEEE Transactions on pattern analysis and machine intelligence*, 27(8):1226–1238, 2005.
- [17] Kun Qian, Takehiro Ando, Kensuke Nakamura, Hongen Liao, Etsuko Kobayashi, Naoki Yahagi, and Ichiro Sakuma. Ultrasound imaging method for internal jugular vein measurement and estimation of circulating blood volume. *International journal of computer assisted radiology and surgery*, 9(2):231–239, 2014.
- [18] J. Ross Quinlan. Induction of decision trees. *Machine learning*, 1(1):81–106, 1986.

- [19] Rangaraj M Rangayyan, Nema M El-Faramawy, JE Leo Desautels, and Onsy Abdel Alim. Measures of acutance and shape for classification of breast tumors. *IEEE Transactions on medical imaging*, 16(6):799–810, 1997.
- [20] Emanuel Rivers, Bryant Nguyen, Suzanne Havstad, Julie Ressler, Alexandria Muzzin, Bernhard Knoblich, Edward Peterson, and Michael Tomlanovich. Early goal-directed therapy in the treatment of severe sepsis and septic shock. *New England Journal of Medicine*, 345(19):1368–1377, 2001.
- [21] Stéfan van der Walt, Johannes L. Schönberger, Juan Nunez-Iglesias, François Boulogne, Joshua D. Warner, Neil Yager, Emmanuelle Gouillart, Tony Yu, and the scikit-image contributors. scikit-image: image processing in Python. *PeerJ*, 2:e453, 6 2014.
- [22] K Sudarshan Vidya, EYK Ng, U Rajendra Acharya, Siaw Meng Chou, Ru San Tan, and Dhanjoo N Ghista. Computer-aided diagnosis of myocardial infarction using ultrasound images with dwt, glcm and hos methods: A comparative study. *Computers in biology and medicine*, 62:86–93, 2015.
- [23] Xiaofeng Yang, Srinu Tridandapani, Jonathan J Beitler, S Yu David, Emi J Yoshida, Walter J Curran, and Tian Liu. Ultrasound glcm texture analysis of radiation-induced parotid-gland injury in head-and-neck cancer radiotherapy: an in vivo study of late toxicity. *Medical physics*, 39(9):5732–5739, 2012.
- [24] Lei Yu and Huan Liu. Feature selection for high-dimensional data: A fast correlation-based filter solution. In *ICML*, volume 3, pages 856–863, 2003.
- [25] Ting Yun and Huazhong Shu. Ultrasound image segmentation by spectral clustering algorithm based on the curvelet and glcm features. In *Electrical and Control Engineering (ICECE), 2011 International Conference on*, pages 920–923. IEEE, 2011.